Series of modulated structures in Sr_xCoO_2 and the modulation rule

L. D. Yao, Y. Q. Guo, J. L. Luo, W. Zhang, F. Y. Li, C. Q. Jin, and R. C. Yu*
Laboratory for Extreme Condition Physics, Beijing National Laboratory for Condensed Matter Physics, Institute of Physics, Chinese Academy of Sciences, P.O. Box 603, Beijing 100080, People's Republic of China
(Received 31 October 2006; revised manuscript received 4 March 2007; published 29 May 2007)

The nominal composition of $Sr_{0.39}CoO_2$, prepared by a low-temperature ion exchange technique, has been systematically studied by transmission electron microscopy, energy dispersive x-ray spectroscopy (EDX), and electron-energy-loss spectroscopy (EELS). Besides a well-defined $\sqrt{3}a_p \times \sqrt{3}a_p$ modulated structure, a series of long periodic modulated structures ($n\sqrt{3}a_p \times 3a_p$) was revealed by high-resolution transmission electron microscopy (HRTEM) in some microzones, which are induced by alternate position ordering of strontium ions. The results of EDX analyses confirm the variation of Sr content in corresponding modulated phases. Moreover, the L_3/L_2 intensity ratio of Co-$L_{2,3}$ edges in the EELS spectra indicates the variation of Co ionic valence state induced by the different contents of Sr cations. Based on the $\sqrt{3}a_p \times \sqrt{3}a_p$ superstructural model, we propose the possible corresponding structural models in this paper. The simulated HRTEM images, based on those models, are consistent with experimental ones. In addition, several phase separations and some structural defects were observed in the sample.

DOI: 10.1103/PhysRevB.75.174118 PACS number(s): 61.72.−y, 72.80.Ga, 61.14.Lj, 61.66.Fn

I. INTRODUCTION

The layered alkali-metal cobalt oxide, such as Li_xCoO_2 ($0.5 \leqslant x \leqslant 1.0$) and Na_xCoO_2 ($0.33 \leqslant x \leqslant 1.0$), has been investigated in the past 20 years due to high mobility of alkali-metal ion and high electronic conductivity. Because it can be used as a cathode material in high-energy-density, reversible solid-state battery systems,[1–3] it has been paid much attention. Recently, broad interest of exploring such high thermoelectric materials has been stimulated since the discovery of a promising thermoelectric material γ-$Na_{0.5}CoO_2$.[4,5] Moreover, Wang *et al.*[6] also reported the surprisingly high thermoelectric power for the metallic conductor $Na_{0.7}CoO_2$. In order to improve thermoelectric properties, Kawata *et al.*[7] tried to partially substitute the sodium site of γ-$Na_{0.55}CoO_2$ with calcium ions to form γ-$Na_{0.55-x}Ca_xCoO_2$ with $0 \leqslant x \leqslant 0.25$. It was observed that there is an obvious enhancement in both Seebeck coefficient and electrical resistivity. As a matter of fact, it is successful in fully replacing alkali-metal ion with divalent alkaline-earth metal ion (Ca^{2+} and Sr^{2+}) for further enhancing thermoelectric properties.[8]

The remarkable structural and chemical characteristics in the alkali-metal cobalt oxide are that the alkali-metal ion content can vary over a large range by intercalation without remarkably modifying the average crystallographic structure. For the Na_xCoO_2 system, it possesses a typical hexagonal crystal structure consisting of layers of Na^+ ions sandwiched between planes of edge shared CoO_6 octahedra. In this structure, it is shown that the Na^+ ions have both trigonal prismatic coordination and octahedral coordination with oxygen between the O-Co-O layers. Prismatic coordination and octahedral coordination occur, as the close-packed oxygen planes directly adjacent to the Na plane have the same projection into the basal plane (*A*-Na-*A*) and have different projections into the basal plane (*A*-Na-*B*), respectively. Thus, on the basis of the various stacking sequences of the oxygen atoms, several average structures have been reported.[3,9–11] Recently, an extensive series of ordered Na-ion–Na-vacancy superlattices was found beyond the simple hexagonal average structure in the Na_xCoO_2 ($0.15 < x < 0.75$) through the study of electron diffraction by Zandbergen *et al.*[12] Surprisingly, the presence of superstructures results from the arrangement of lines of Na ions and vacancies rather than simply maximized Na-Na separations. It is interesting that these superstructures can be affected by electron-beam irradiation, owing to high mobility of Na ions. For the series of M_xCoO_2 (M=Ca or Sr) materials, they are expected to be more stable than their analogous Na_xCoO_2 materials due to the greater electrostatic interaction between divalent ions and the negative CoO_2 layer, which makes $(Sr,Ca)_xCoO_2$ more suitable for transmission electron microscopy (TEM) observations. The average structure of M_xCoO_2 (M=Ca or Sr) is similar to the hexagonal average structure of A_xCoO_2 (A=Na or Li). However, though there are two possible strontium and/or calcium sites, 2*b* (0,0,1/4) and 2*d* (2/3,1/3,1/4), the strontium and/or calcium ions occupy only the 2*d* sites according to the calculative results of Madelung potential for the Sr_xCoO_2.[8] Recently, two superstructures in $Sr_{0.35}CoO_2$ arising, respectively, from the intercalated Sr ordering (a compositional modulation) with $\mathbf{q}_1 = \mathbf{a}^*/3 + \mathbf{b}^*/3$ and a periodic structural distortion (a transverse structure modulation) $\mathbf{q}_2 = \mathbf{a}^*/2$ were observed by Yang *et al.*[13] In this paper, we report a series of modulated structures induced by alternate position ordering of strontium ions in the nominal $Sr_{0.39}CoO_2$, which are obtained from the high-resolution transmission electron microscopy (HRTEM) observations.

II. SAMPLE PREPARATION

Polycrystalline samples of nominal $Sr_{0.39}CoO_2$ were synthesized by a low-temperature ion exchange technique from $Na_{0.78}CoO_2$ precursor. The ion exchange process was similar to those reported by Cushing and Wiley.[14] The polycrystalline precursor, $Na_{0.78}CoO_2$, was prepared from Na_2CO_3 and Co_3O_4 by a conventional solid-state reaction. The well-mixed powders were heated at 750 °C for 12 h, and were

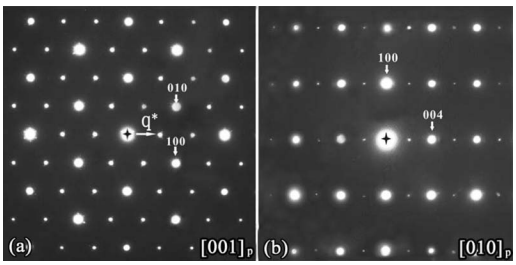

FIG. 1. Selected area ED patterns of $Sr_{0.39}CoO_2$ along the (a) [001] and (b) [010] zone-axes.

then reground and heated at 850 °C for 24 h. The detailed process was mentioned in Ref. 15. Thin foils for TEM studies were prepared by crushing the bulk specimen in an agate mortar filled with alcohol, and then dispersing the fine fragments suspended in alcohol on a microgrid. A Tecnai F20 field-emission electron microscope installed at Beijing Laboratory of Electron Microscopy, Beijing National Laboratory for Condensed Matter Physics, was used for electron diffraction (ED), HRTEM, energy dispersive x-ray spectroscopy (EDX), and electron-energy-loss spectroscopy (EELS) experiments. All the TEM studies were carried out at an acceleration voltage of 200 kV.

III. RESULTS AND DISCUSSION

According to the analysis of x-ray-diffraction (XRD) pattern reported by Guo *et al.*,[15] the nominal composition $Sr_{0.39}CoO_2$ is isomorphic to γ-Na_xCoO_2 and the diffraction peaks can be indexed to a hexagonal unit cell with a space group of $P6_3/mmc$. Compared with the lattice parameters of the precursor, we find that for the $Sr_{0.39}CoO_2$, the lattice parameter $\boldsymbol{c}_p$ (hereinafter the subscript p stands for the primitive structure) becomes lengthened, while the $\boldsymbol{a}_p$ axis becomes slightly shortened. This result can be ascribed to the fact that the ionic radius of Sr^{2+} is larger than Na^+.

Through XRD analyses, the average structure of the sample can be determined. However, TEM observations may offer much information of local structures, such as superstructures, phase separation, structural defects, etc. In the nominal composition of $Sr_{0.39}CoO_2$, we found a series of modulated structures in some microzones through HRTEM observations.

A. Basic modulated structure

In the nonstoichiometric compound Sr_xCoO_2, it is generally reported that the well-defined $\sqrt{3}a_p \times \sqrt{3}a_p$ superstructure is formed due to Sr ionic ordering. In our $Sr_{0.39}CoO_2$, we also observed the same modulated structure. Here, it is called as basic modulated structure. In Figs. 1(a) and 1(b), the ED patterns of the sample are shown along the $[001]_p$ and $[010]_p$ zone axes, respectively. The diffraction spots with strong intensity can be well indexed to a hexagonal unit cell with lattice parameters $\boldsymbol{a}_p$=0.282 nm and $\boldsymbol{c}_p$=1.152 nm and a space group of $P6_3/mmc$ with the reflection conditions of $l=2n$ for $(h\ h\ l)$, $l=2n$ for $(2h\ -h\ l)$, and $l=2n$ for $(h\ -2h\ l)$. However, in Fig. 1(a), it can be seen that the weak

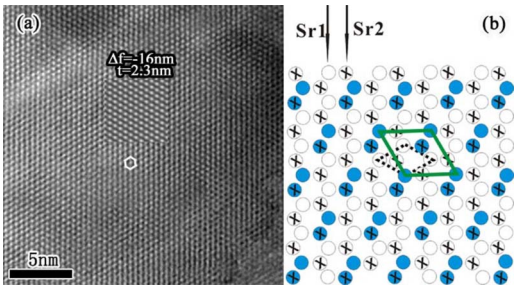

FIG. 2. (Color online) (a) HRTEM image of $\sqrt{3}a_p \times \sqrt{3}a_p$ modulated phase along the $[001]_p$ zone axis. (b) The corresponding structure model in $\mathbf{a}_p$-$\mathbf{b}_p$ plane, where occupied Sr positions are given as filled circles (blue ones in color figure) and Sr vacancies by open circles. Sr1 and Sr2 denote the upper and lower layer Sr atom planes in a unit cell, respectively. The symbol X indicates the positions of the underlying Sr atoms. The primitive hexagonal unit cell is indicated by dotted lines (black ones in color figure), while the basic hexagonal supercell is marked by solid lines (green ones in color figure).

diffraction spots appear along the $\langle 110 \rangle$ direction. The superstructure reflections can be described by wave vector $\mathbf{q}^*$ $(1/3,1/3,0)$, which is along the $\langle 110 \rangle_p^*$ direction with a length of $[110]_p^*/3$. In real space, $1/\mathbf{q}^*$ has a length of $\sqrt{3}d(110)_p$. So, the superstructure unit cell can be defined as $\sqrt{3}a_p \times \sqrt{3}a_p$ within the basic $\mathbf{a}_p$-$\mathbf{b}_p$ plane.

Figure 2(a) shows a typical HRTEM image of the basic superstructure taken along $[001]_p$ zone axis, where a supercell is outlined by white solid lines. As is well known, the superstructure results from the Sr ionic ordering in $2d$ sites according to the rule of maximized Sr-Sr separations.[13] In order to further display the distribution of Sr ions, a model for the stacking along the c axis of the superstructure is given in Fig. 2(b). In this model, we only draw planes with Sr atoms perpendicular to the $[001]_p$ direction, where occupied Sr positions are given as filled circles (blue ones in color figure) and Sr vacancies by open circles. Sr1 and Sr2 denote the upper layer and the lower layer Sr atom planes in a unit cell, respectively. The symbol X indicates the positions of the underlying Sr atoms. From the schematic model, it is illustrated that the neighboring Sr atoms in the same plane do not occupy the nearest sites, but the next-nearest sites. Thus, the arrangement of Sr ions submits to the fact that the Sr-Sr distances are as large as possible and results in the formation of the basic modulated structure. The basic hexagonal unit cell is indicated by dotted lines (black ones in color figure), while the supercell is marked by solid lines (green ones in color figure). Based on the proposed model, HRTEM images are simulated by using the simulation program JEMS.[16] A simulated image for a defocus value of −16 nm and a thickness of 2.3 nm, embedded in the image, appears to be in good agreement with the experimental one. In this superstructure, it is calculated that the occupancy ratio of Sr ions is 0.33, which suggests the reason why the well-defined Sr-ordered state tends to appear at $x \approx 1/3$ in the Sr_xCoO_2 materials. In fact, the results of EDX analyses show that the metal ratio (Sr:Co) is close to 0.33 in this corresponding modulated phase.

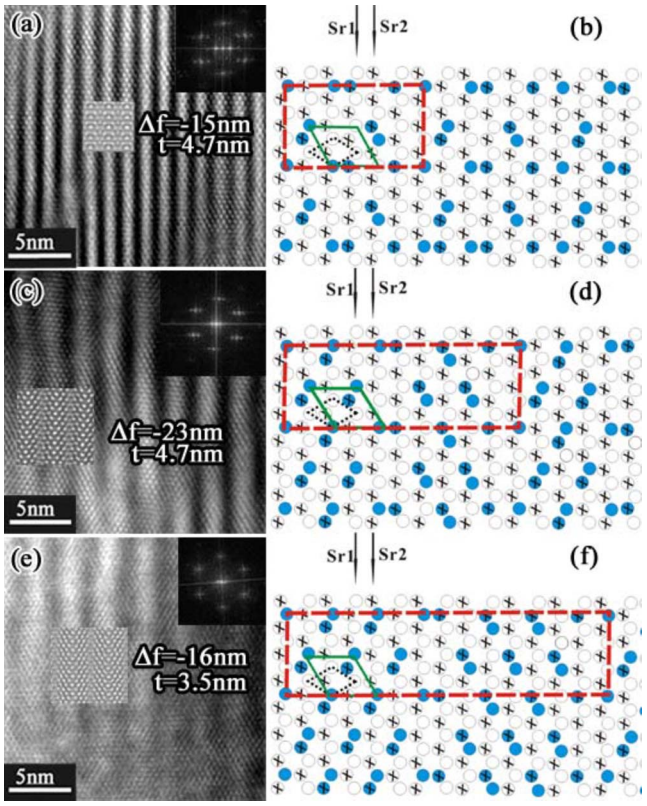

FIG. 3. (Color online) (a), (c), and (e) are the HRTEM images of $3\sqrt{3}a_p\times 3a_p$, $5\sqrt{3}a_p\times 3a_p$, and $7\sqrt{3}a_p\times 3a_p$ modulated phases along the $[001]_p$ zone axis, respectively. (b), (d), and (f) are the corresponding structure models in $\mathbf{a}_p$-$\mathbf{b}_p$ plane, where the supercell is marked by dashed lines (red ones in color figure).

B. $n\sqrt{3}a_p\times 3a_p$ modulated structures

For the Sr_xCoO_2 materials, it is believed that different concentrations and ordering states of Sr cation can lead to complex inhomogeneities and phase separation. For instance, the compositional inhomogeneities in microzone may appear due to the high Sr doping level in the nominal composition $Sr_{0.39}CoO_2$. We observed in this sample several remarkable modulated structures corresponding to different Sr contents and ordering states in some microzones besides the basic modulated structure from the HRTEM studies. In Figs. 3(a), 3(c), and 3(e), several typical modulated structure images taken along the $[001]_p$ zone axis are presented.

In Fig. 3(a), a wavy HRTEM image can be seen, where the periodicity of modulation along the $[100]_m$ (hereinafter, the subscript m stands for the basic modulated structure) direction is $3\sqrt{3}a_p$. The fast Fourier transform (FFT) patterns corresponding to the modulation phase are shown on the top right corner. In view of the feature of the HRTEM image, it is concluded that the modulated structure can be induced by alternate position ordering of Sr cations on the basis of the basic modulated structure. The structure model proposed in the $\mathbf{a}_p$-$\mathbf{b}_p$ planes is shown in Fig. 3(b). In this model, the $\sqrt{3}a_p\times 3a_p$ block, like that in the basic modulated structure, is adjacent to the reverse block along the $[100]_m$ direction, i.e., in the former block, the Sr ion distribution in the upper and lower layers is opposite to those in the latter blocks, while the distribution rule of Sr ions is the same as that in the basic modulated structure along the $[120]_m$ direction. In addition, the Sr ions do not yet occupy the nearest neighboring sites in order to reach a low-energy state of the system. It is very clear that the crystal structure varies from a hexagonal one for the basic modulated structure to an orthorhombic one for the new modulated structure. Thus, the supercell can be described as $\boldsymbol{a}_{m1}=3\sqrt{3}\,\boldsymbol{a}_p$, $\boldsymbol{b}_{m1}=3\boldsymbol{a}_p$, and $\boldsymbol{c}_{m1}=\boldsymbol{c}_p$, in which the occupancy ratio of Sr cations is close to 0.22.

Besides the above-mentioned modulated structure, we also observed some microzones exhibiting a series of superstructures similar to $3\sqrt{3}a_p\times 3a_p$ modulated structure. Figures 3(c) and 3(e) display two HRTEM images taken along the $[001]_p$ zone axis, with modulated lengths of $5\sqrt{3}a_p$ and $7\sqrt{3}a_p$ along the $[100]_m$ direction, respectively. Accordingly, two structure models are proposed on the basis of alternate position ordering of Sr cations, as shown in Figs. 3(d) and 3(f). The similar distribution rules of Sr cations are used in the two models. However, it should be pointed out that the reverse blocks along the $[100]_m$ direction should be taken as $2\sqrt{3}a_p\times 3a_p$ (or $3\sqrt{3}a_p\times 3a_p$) for the $5\sqrt{3}a_p\times 3a_p$ (or $7\sqrt{3}a_p\times 3a_p$) modulated structure. According to the models in Figs. 3(c) and 3(e), the supercells are marked by dashed lines (red ones in color figures), with lattice parameters $\boldsymbol{a}_{m2}=5\sqrt{3}\,\boldsymbol{a}_p$, $\boldsymbol{b}_{m2}=3\boldsymbol{a}_p$, and $\boldsymbol{c}_{m2}=\boldsymbol{c}_p$ and $\boldsymbol{a}_{m3}=7\sqrt{3}\,\boldsymbol{a}_p$, $\boldsymbol{b}_{m3}=3\boldsymbol{a}_p$, and $\boldsymbol{c}_{m3}=\boldsymbol{c}_p$, respectively. The occupancy ratios of Sr cations are close to 0.27 and 0.29, respectively, in the supercells.

Based on the analyses of the above-mentioned modulated structures, we propose a modulation rule for the series of modulated structures. This series of modulated structures has an orthorhombic form of $n\sqrt{3}a_p\times 3a_p$ with a modulated periodicity of $n\sqrt{3}a_p$, where n is an odd number and $n\geqslant 3$, along the $[100]_m$ direction. These modulated phases are induced by the alternate position ordering of strontium ions, i.e., there is a reverse distribution of Sr ions between the neighboring $[(n-1)/2]\sqrt{3}a_p\times 3a_p$ blocks along the $[100]_m$ direction. In addition, the occupancy of Sr ions should follow a principle that two Sr ions do not yet occupy the nearest neighboring sites in order to reach low systemic energy. Based on this modulation rule, the structure with $n=\infty$ corresponds to the basic modulated structure. In this case, the orthorhombic structure type transforms to the hexagonal one.

Obviously, except the basic modulation phase, the series of the observed modulation phases all possess orthorhombic structures. So, it is evident that the alternate position ordering arrangement of Sr cations lowers the symmetry of the original structure. In order to examine the correctness of our proposed modulation rule, we carried out HRTEM image simulations. Based on the above proposed structure models, the simulated images along the $[001]_p$ zone axis are embedded in Figs. 3(a), 3(c), and 3(e), respectively. It is clear that the simulated images are in good agreement with the experimental ones, indicating that the proposed structure models are reasonable and our proposed modulation rule is correct. However, it should be noted that those are only idealized structure models, since the alternate position ordering arrangement of Sr cations will lightly adjust the positions of Co and O atoms and inevitably lead to lattice distortion. So, more precise crystallographic data of those modulated struc-

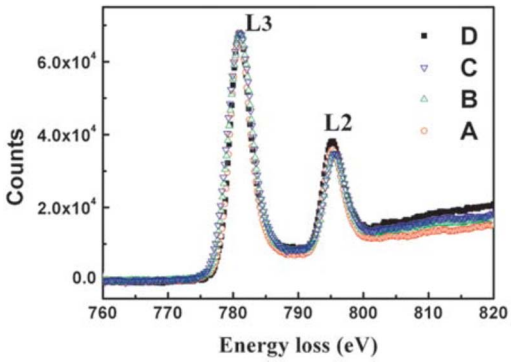

FIG. 4. (Color online) Normalized EELS spectra including Co-$L_{2,3}$ edges obtained from different modulated phases along the $[001]_p$ zone-axis direction, where A, B, C, and D denote $\sqrt{3}a_p \times \sqrt{3}a_p$, $7\sqrt{3}a_p \times 3a_p$, $5\sqrt{3}a_p \times 3a_p$, and $3\sqrt{3}a_p \times 3a_p$, respectively.

tures should be determined by XRD or neutron-diffraction experiments after a pure single modulated phase is synthesized. Unfortunately, in our samples, those modulated phases appear in some microzones with the scale of nanometers.

With the increase of n, the occupancy ratio of Sr cations in the supercell gradually increases and closes to 0.33 for $n=\infty$. EDX results confirmed the variation of Sr content in different modulated phases and show good agreement with theoretical calculations. On the other hand, EELS supplies indirect evidence of the variation of Co ionic valence state, since Co ionic valence falls with the increase of Sr content. Figure 4 shows the EELS spectra including Co-$L_{2,3}$ absorption edges obtained from several modulated phases along the $[001]_p$ zone-axis direction. We normalized all the spectra in Fig. 4 to have the same Co-L_3 edge integrated counts. By comparing the Co-$L_{2,3}$ edges, one can see that the L_3/L_2 intensity ratio falls with the increase of modulated length, indicating that cobalt ions in the basic modulated phase show up a lower valence state according to the well-known relationship between the L_3/L_2 intensity ratio and the valence state for Co ions.[17]

C. Phase separation and structural defects

As mentioned above, the orderings of Sr cations can induce different modulated structures, but on, the other hand, a certain extent of inhomogeneity of the Sr cations can bring about phase separation and structural defects. In our experiments, the coexistence of two phases and multiphases as well as some typical structural defects was observed in some areas.

Figure 5(a) shows a HRTEM image taken along the $[001]_p$ zone axis, which indicates a coexistence of two phases, i.e., the basic modulated phase coexisting with the $5\sqrt{3}a_p \times 3a_p$ modulated phase. The domains A and B refer to the former and the latter ones, respectively, as suggested by their corresponding FFTs given in Fig. 5(a). Besides the coexistence of two phases, the coexistence of multiphases was also observed as shown in Fig. 5(b), where the domains A, B, C, and D stand for $5\sqrt{3}a_p \times 3a_p$, $7\sqrt{3}a_p \times 3a_p$, $9\sqrt{3}a_p \times 3a_p$, and $5\sqrt{3}a_p \times 3a_p$ modulated phases, respectively, according

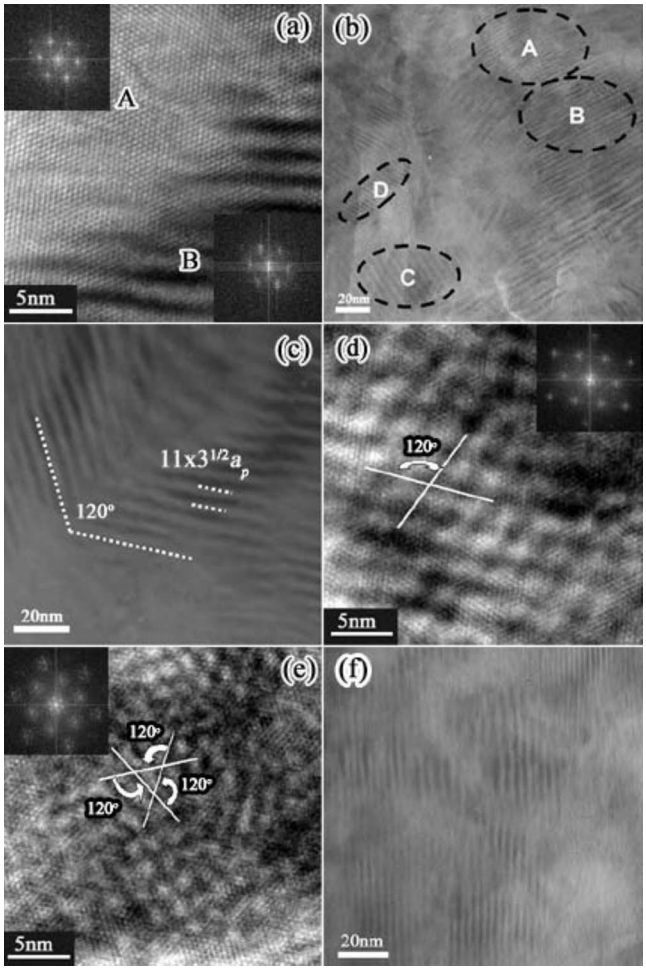

FIG. 5. (a) HRTEM image of the coexistence of two phase domains taken along the [001] zone axis, where the domains A and B refer to the basic modulated phase and $5\sqrt{3}a_p \times 3a_p$ modulated phase, respectively. The corresponding FFT patterns are shown in the top left and foot right corners, respectively. (b) TEM image of multiphase coexistence domain, where the domains A, B, C, and D stand for $5\sqrt{3}a_p \times 3a_p$, $7\sqrt{3}a_p \times 3a_p$, $9\sqrt{3}a_p \times 3a_p$, and $5\sqrt{3}a_p \times 3a_p$ modulated phases, respectively. (c) TEM image of a typical twinning boundary in the $11\sqrt{3}a_p \times 3a_p$ modulated phase. (d) HRTEM image of a structure modulated in two directions with an angle of 120° and a wavelength of $5\sqrt{3}a_p \times 3a_p$. The corresponding FFT pattern is shown at the top right corner. (e) HRTEM image of a structure modulated in three directions with an angle of 120° between any two directions and a wavelength of $3\sqrt{3}a_p \times 3a_p$. The corresponding FFT pattern is shown at the top left corner. (f) TEM image of an area with some modulated phases at low temperature.

to the measured modulated length. No changes were observed during exposing to the electron beam, indicating that the coexistences exist in the sample from the beginning. In addition, some twinning boundaries were occasionally seen in some areas, especially in $n\sqrt{3}a_p \times 3a_p$ modulated phases. Figure 5(c) shows a typical twinning boundary in the $11\sqrt{3}a_p \times 3a_p$ modulated phase. Because there is an angle of 120° between two grains, the boundary of the twins lies in a definite $(\underline{1}1\underline{3}0)$ atomic plane of the $11\sqrt{3}a_p \times 3a_p$ modulated structure. More interestingly, some structures modulated in two directions with an angle of 120° were observed in our

sample, and a HRTEM image along the $[100]_m$ zone axis is presented in Fig. 5(d). The corresponding FFT pattern is shown at the top right corner. It is seen that the modulated wavelength in both directions is $5\sqrt{3}a_p \times 3a_p$. Moreover, some structures that are modulated in three directions with an angle of 120° between any two directions were also observed in some microzones. Figure 5(e) shows such a modulated structure taken along the $[100]_m$ zone axis, which has a modulated wavelength of $3\sqrt{3}a_p \times 3a_p$ in three directions, and the corresponding FFT pattern is displayed at the top right corner. Here, it should be noted that the Sr content is very low in such modulated phases. In order to explore the influence of temperature on the distribution of Sr cations, we carried out TEM observations at low temperature (about 80 K). A TEM image in Fig. 5(f) shows that all modulated phases and structural defects are invariable with decreasing temperature, indicating that the ordering state of Sr cations is not influenced by such low temperatures.

For a series of Sr_xCoO_2 materials, the value of x influences the Co^{3+}/Co^{4+} ratio (i.e., for the hypothetical composition $x=0$, all Co^{4+} would be found, and for hypothetical $x=0.5$, all Co^{3+} would be found), further on the physical properties, because the electrical transport property is mainly ascribed to the movement of $3d$ orbital electrons in Co ions for this system materials. However, the presence of different types of the Sr ion ordering over the available sites will also play an important role in the physical properties. In the basic modulated phase, both Co^{3+} and Co^{4+} ions show homogeneous distribution in the $\mathbf{a}_p$-$\mathbf{b}_p$ plane, and the average valence of Co ions is close to +3.33, whereas the valence of Co ions deviates from the value of +3.33 and tends to rise near the reverse planes in $n\sqrt{3}a_p \times 3a_p$ modulated phases in view of the distribution of Sr atoms in corresponding structure models. Therefore, the electronic transport property in this series of modulated phases would represent obvious anisotropy in the $\mathbf{a}_p$-$\mathbf{b}_p$ plane, i.e., the conductivity along the $[120]_m$ direction would be different from the one along $[100]_m$.

IV. CONCLUSIONS

In summary, polycrystalline sample of $Sr_{0.39}CoO_2$, prepared by the low-temperature ion exchange technique, is isomorphic to γ-Na_xCoO_2 with a layered hexagonal structure. A systematic study of microstructure through TEM observations reveals that all kinds of the orthorhombic modulated phases appear in some microzones. Besides the typical basic modulated structure $\sqrt{3}a_p \times \sqrt{3}a_p$, a series of modulated structures with $n\sqrt{3}a_p \times 3a_p$, where n is an odd number and more than or equal to 3, was found by HRTEM observations. We proposed a modulation rule and concluded that those modulated phases are induced by the alternate position ordering of strontium ions, i.e., there is a reverse distribution of Sr ions between two neighboring $[(n-1)/2]\sqrt{3}a_p \times 3a_p$ blocks along the $[100]_m$ direction. Moreover, the occupancy of Sr ions should follow a principle that two Sr ions do not yet occupy the nearest neighboring sites in order to reach low systemic energy. Following our proposed modulation rule, the basic modulated structure corresponds to the case of $n=\infty$. The EDX results confirm the variation of Sr content in corresponding modulated phases. In addition, the Co-$L_{2,3}$ EELS results indicate the variation of Co ionic valence state induced by the different contents of Sr cations. Phase separation and structural defects exist in certain microzones.

ACKNOWLEDGMENTS

This work was supported by the National Natural Science Foundation of China (Grant Nos. 50471053, 50321101, 10674166, and 50332020) and the State Key Development Program for Basic Research of China (Grant Nos. 2005CB623602 and 2005CB724402).

*Corresponding author.

[1] J. Molenda, C. Delmas, and P. Hagenmuller, Solid State Ionics **10**, 431 (1983).
[2] M. G. S. R. Thomas, P. G. Bruce, and J. B. Goodenough, Solid State Ionics **17**, 13 (1985).
[3] Y. Ono, R. Ishikawa, Y. Miyazaki, Y. Ishii, Y. Morii, and T. Kajitani, J. Solid State Chem. **166**, 177 (2002).
[4] I. Terasaki, Y. Sasago, and K. Uchinokura, Phys. Rev. B **56**, R12685 (1997).
[5] A. C. Masset, C. Michel, A. Maignan, M. Hervieu, O. Toulemonde, F. Studer, B. Raveau, and J. Hejtmanek, Phys. Rev. B **62**, 166 (2000).
[6] Y. Y. Wang, N. S. Rogado, R. J. Cava, and N. P. Ong, Nature (London) **423**, 425 (2003).
[7] T. Kawata, Y. Iguchi, T. Itoh, K. Takahata, and I. Terasaki, Phys. Rev. B **60**, 10584 (1999).
[8] R. Ishikawa, Y. Ono, Y. Miyazaki, and T. Kajitani, Jpn. J. Appl. Phys., Part 2 **41**, L337 (2002).
[9] C. Delmas, J. J. Braconnier, C. Fouassier, and P. Hagenmuller, Solid State Ionics **3-4**, 165 (1981).
[10] C. Fouassier, G. Matejka, J.-M. Reau, and P. Hagenmuller, J. Solid State Chem. **6**, 532 (1973).
[11] R. J. Balsys and R. L. Davis, Solid State Ionics **93**, 279 (1996).
[12] H. W. Zandbergen, M. L. Foo, Q. Xu, V. Kumar, and R. J. Cava, Phys. Rev. B **70**, 024101 (2004).
[13] H. X. Yang, Y. G. Shi, Y. Q. Guo, X. Liu, R. J. Xiao, J. L. Luo, and J. Q. Li, Mater. Res. Bull. **42**, 94 (2007).
[14] B. L. Cushing and J. B. Wiley, J. Solid State Chem. **141**, 385 (1998).
[15] Y. Q. Guo, J. L. Luo, G. T. Liu, H. X. Yang, J. Q. Li, N. L. Wang, D. Jin, and T. Xiang, Phys. Rev. B **74**, 155129 (2006).
[16] P. Stadelmann, JEMS, electron microscopy software, Java version, CIME-EPFL, Switzerland, 1999.
[17] Z. L. Wang, J. S. Yin, and Y. D. Jiang, Micron **31**, 571 (2000).